Rare Metal Materials and Engineering
Volume 51, Issue 7, July 2022
Available online at www.rmme.ac.cn

Science Press

Cite this article as: Zhao Hui, Yang Chong, Guo Dongxu, et al. Thermomechanical Response Simulation of FeCrAl and Zr-2 Fuel Claddings Under Neutron Irradiation[J]. Rare Metal Materials and Engineering, 2022, 51(07): 2460-2466.

ARTICLE

Thermomechanical Response Simulation of FeCrAl and Zr-2 Fuel Claddings Under Neutron Irradiation

Zhao Hui[1], Yang Chong[1], Guo Dongxu[1], Wu Lu[2], Pan Rongjian[2], Qin Jiantao[2], Shi Baodong[1]

[1] National Engineering Research Center for Equipment and Technology of Cold Rolled Strip, School of Mechanical Engineering, Yanshan University, Qinhuangdao 066004, China; [2] State Key Laboratory of Nuclear Fuel and Materials, The First Sub-Institute, Nuclear Power Institute of China, Chengdu 610041, China

Abstract: The representative C35M alloy among FeCrAl alloys was selected as the research object, and a small fuel rod model was established. Based on the user material (UMAT) subroutine, the radiation creep model of the C35M alloy was embedded in the subroutine. The thermomechanical coupling behavior of C35M alloy under neutron irradiation was calculated by the finite element software ABAQUS. Using Zr-2 alloy as a comparison, the evolution of the distribution of the temperature field, stress field, displacement field, and gap distance of the cladding over time of the alloys was analyzed. Results show that the temperature field and the stress field of the two alloys are basically the same. The temperature distribution is mainly affected by the coolant, while the stress field is related to the temperature and creep rate. During the simulation, the Zr-2 alloy mainly grows through irradiation, while C35M alloy shows the irradiation creep and has a little thermal expansion deformation. The gap closure rate of Zr-2 alloy is much faster than that of C35M alloy, which indicates that C35M alloy can prolong the accident response time. However, in order to adapt to the complex environment in the reactor, the material still needs to be optimized to improve its strength and creep rate.

Key words: neutron irradiation; irradiation creep; FeCrAl; Zr-2; cladding

In the normal operation of nuclear reactors, the cladding is subjected to a complex working environment. The inner wall interacts with the fuel pellets, which is prone to cracking. The outer wall is subjected to high temperature, high pressure, neutron irradiation, and direct contact with the coolant, which is prone to chemical corrosion[1]. The selection of cladding materials is critical to the safety of nuclear reactors[2]. Due to their excellent mechanical properties and corrosion resistance, Zr alloys are applied to cladding tubes of fuel rods for nuclear reactor[3]. However, in the Fukushima incident, the zirconium alloy cladding of the fuel assembly had a violent oxidation reaction with the high-temperature water vapor, leading to the melting of the reactor core and the hydrogen explosion, and causing a serious nuclear accident. Therefore, it is necessary to develop the new materials for high performance requirements under severe conditions.

FeCrAl alloys attract much attention due to their excellent resistance to high temperature water vapor oxidation, stable thermophysical properties, and good radiation resistance[4-9]. Currently, FeCrAl alloys are mainly used in the fossil fuel power plants[10], and cannot fully adapt to the complex working conditions in the reactor. The composition and performance of FeCrAl alloys are still in the research stage. Simulation is an effective way for material development and testing. Through the simulation, the material development period can be shortened, and the material performance can be predicted. As the FeCrAl alloy cladding is a novel fuel cladding, few specific supporting programs exist for engineering calculations[11]. The commercially available ABAQUS software provides a reasonable general framework

Received date: July 13, 2021
Foundation item: National Natural Science Foundation of China (51771166); Natural Science Foundation of Hebei Province (E2019203452, E2021203011); Talent Project of Human Resources and Social Security Department of Hebei Province (A202002002); Central Government Guiding Local Science and Technology Development Project (216Z1001G); Key Project of Department of Education of Hebei Province (ZD2021107); Sponsored by State Key Laboratory of Materials Processing and Die & Mould Technology, Huazhong University of Science and Technology (P2020-013)
Corresponding author: Shi Baodong, Ph. D., Professor, National Engineering Research Center for Equipment and Technology of Cold Rolled Strip, School of Mechanical Engineering, Yanshan University, Qinhuangdao 066004, P. R. China, Tel: 0086-335-8387652, E-mail: baodong.shi@ysu.edu.cn

for fuel performance modeling[12,13] in order to analyze the deformation and thermomechanical behavior of the cladding with empirical models[14,15]. However, as a conceptual cladding material, the behavior of FeCrAl alloys in the reactor is still unclear. Besides, it is difficult to obtain the real-time status of the cladding material in the reactor during operation process, so the simulation is crucial to predict and verify the reactor fuel element behavior in the reactor. The thermomechanical behavior of FeCrAl alloys under neutron irradiation was studied by ABAQUS. In this research, the Zr-2 alloy and representative C35M alloy of the FeCrAl alloys were used for comparison analysis. The user-defined subroutine was used to embed the empirical formula of the two alloys to study the effect of neutron irradiation on the mechanical and thermal properties of FeCrAl alloys, which provides a reference for the further improvement of the properties of FeCrAl alloys.

1 Material and Simulation Model Establishment

The materials of cladding tubes were cold-worked Zr-2 alloy and C35M wrought alloy in this research. The core block material was UO_2. In the normal operation, the heat is transferred from the center of the UO_2 pellet to the inner wall of the cladding, and then is spread along the radial directions of the cladding. Under the influence of temperature and neutron irradiation, the properties of the cladding changed during operation, affecting the performance and service life of fuel rods. Therefore, an effective model involving the physical parameters with temperature is important to analyze the thermal behavior of materials.

1.1 Thermophysical properties of UO_2 pellet

The heat transfer coefficient of UO_2 fuel was calculated using the Lucita modified model[16], which comprehensively considers the effects of temperature, burnup, fuel fission products, and porosity on the heat transfer coefficient, as follows:

$$k_{UO_2} = k_{95} F_D F_P F_M F_R \quad (1)$$

where k_{95} is the thermal conductivity of unirradiated UO_2 at 95% theoretical density ($W \cdot m^{-1} \cdot K^{-1}$); F_D and F_P are the influencing factors of dissolved and precipitated thermal fission products, respectively; F_R and F_M are the influence factors of irradiation effect and porosity, respectively. k_{95}, F_D, F_P, F_R, and F_M can be expressed by Eq.(2~6), respectively, as follows:

$$k_{95} = \frac{1}{0.041 + 2.165 \times 10^{-4} T + (1 + 396 e^{-6380/T})^{-1}} + \left[\frac{4.715 \times 10^9}{T^2}\right] \exp\left(-\frac{16\,361}{T}\right) \quad (2)$$

$$F_D = \left[\frac{1.09}{B^{2.265}} + \frac{0.0643}{B}\sqrt{T}\right] \arctan\left(\frac{1.09}{B^{2.265}} + \frac{0.0643}{B}\sqrt{T}\right)^{-1} \quad (3)$$

$$F_P = 1 + \left(\frac{0.019B}{3 - 0.019B}\right)\left[1 + \exp\left(\frac{1200 - T}{100}\right)\right]^{-1} \quad (4)$$

$$F_R = 1 - \frac{0.019B}{1 + \exp\left(\frac{T - 900}{80}\right)} \quad (5)$$

$$F_M = \frac{1 - P}{1 + (s - 1)P} \quad (6)$$

where T is temperature (K); B is fuel consumption of the fuel system (in this research, B=50%); P is the porosity; s is the shape factor of the sphere (in this research, s=0.5).

The relationship between the thermal expansion coefficient of UO_2 fuel and temperature can be expressed as follows:

$$\frac{\Delta L}{L} = K_1 T - K_2 + K_3 \exp\left(\frac{E_D}{KT}\right) \quad (7)$$

where K_1=1.0×10^{-5} K^{-1}; K_2=3.0×10^{-3} K^{-1}; K_3=4.0×10^{-2} K^{-1}; L is the vertical length of UO_2 fuel; K and E_D are the Boltzmann constant and thermodynamic parameter of the system, respectively (in this research, E_D=6.9×10^{-20} J and K=1.38×10^{-23} J/K).

The density and Poisson's ratio of UO_2 fuel are 10.96 g/cm^3 and 0.316, respectively.

1.2 Thermophysical properties of Zr-2 alloy

The thermal conductivity of Zr-2 alloy (k_{Zr}, $W \cdot m^{-1} \cdot K^{-1}$) was established, which is related to the temperature and can be obtained through the experiment data from Ref. [17], as follows:

$$k_{Zr} = 19.25 - 0.021T + 7.54 \times 10^{-5} (T + 273)^2 \quad T < 670 \text{ K} \quad (8)$$

The Young's modulus of Zr-2 alloy (E_{Zr}, GPa) is also related to the temperature[18] and can be expressed as follows:

$$E_{Zr} = 97.08 - 0.058 \times (T - 273) \quad T < 1090 \text{ K} \quad (9)$$

The irradiation growth and creep of the cladding tubes are induced by the neutron irradiation, which is affected by the fast neutron fluence rate. An empirical model is employed to evaluate the radiation growth (ε_g) performance of cladding in steady state[19], as follows:

$$\varepsilon_g = A_g (\phi t)^{n_g} \quad (10)$$

where ϕ is the fast neutron fluence rate ($n \cdot m^{-2} \cdot s^{-1}$); A_g and n_g are the material constants (A_g=3×10^{-20} n·cm^{-2} and n_g=0.794); t is the time.

The creep behavior of cladding is composed of thermal creep and radiation creep. The radiation creep of Zr-2 alloy is induced by neutron irradiation. The Hoop model was used to calculate the irradiation creep, which is related to the stress and fast neutron fluence rate[20]. The effective irradiation creep rate of Zr-2 alloy can be expressed as follows:

$$\dot{\varepsilon}_{irr}^{Zr} = C_0 \phi^{C_1} \sigma_M^{C_2} \quad (11)$$

where σ_M is the Mises stress (MPa); C_0, C_1, and C_2 are the material constants of 9.881×10^{-28}, 0.85, and 1.0, respectively. The material model was implemented in the User Material (UMAT) subroutine in ABAQUS.

The thermal creep rate of Zr-2 alloy can be calculated by Eq.(12), as follows:

$$\dot{\varepsilon}_{thermal}^{Zr} = A_0 \left(\frac{\sigma_M}{G}\right)^n \exp\left(\frac{-Q}{RT}\right) \quad (12)$$

where G is the shear modulus (MPa); Q is the activation energy (270 kJ/mol); R is the gas constant ($J \cdot mol^{-1} \cdot K^{-1}$); A_0 and n are material parameters (n=5 and A_0=3.14×10^{-24} $MPa^{-1} \cdot s^{-1}$).

Therefore, the creep rate of Zr-2 alloy can be described as follows:

$$\dot{\varepsilon}^{Zr} = \dot{\varepsilon}^{Zr}_{irr} + \dot{\varepsilon}^{Zr}_{thermal} \quad (13)$$

The density and Poisson's ratio of Zr-2 alloy are 6.55 g/cm^3 and 0.42, respectively.

1.3 Thermophysical properties of C35M alloy

The thermal conductivity of C35M alloy was tested by Oak Ridge National Laboratory (ORNL)[21], and the fitting relationship was obtained, as follows:

$$k_{C35M} = -19.86 \times 10^{-7}T^2 + 1.537 \times 10^{-2}T + 8.502 \quad (14)$$

where k_{C35M} is the thermal conductivity of C35M alloy (W·m^{-1}·K^{-1}).

The specific heat capacity of C35M alloy can be obtained by Eq.(15)[21], as follows:

$$C_{C35M} = aT + bT^2 + cT^3 \quad (15)$$

where C_{C35M} is specific heat (J·kg^{-1}·K^{-1}); a, b, and c are fitting parameters. When the temperature is lower than 870 K, a=2.45, b=−4.002×10^{-3}, and c=2.72×10^{-6}.

The density of C35M alloy is 7.06 g/cm^3. The generalized empirical relationship between the Poisson's ratio and temperature of C35M alloy can be described by Eq. (16)[22], as follows:

$$v = 4.46 \times 10^{-5}(T + 273) + 0.27 \quad (16)$$

By measuring the elastic modulus of different FeCrAl alloys, Thompson et al[23] detected that the composition change will not affect the change of elastic modulus. The elastic modulus of the wrought FeCrAl alloys is at least twice larger than that of the Zr-based alloys. The elastic modulus of C35M alloy can be calculated by Eq.(17), as follows:

$$E_{C35M} = 199 - 5.46 \times 10^{-5}T^2 - 3.85 \times 10^{-2}T \quad (17)$$

Yamamoto et al[21] tested the thermal expansion of different types of FeCrAl alloys and found that when the temperature is below 1000 K, the coefficient of thermal expansion of alloys will be slightly different; when the temperature continues to rise, the difference in the coefficient of thermal expansion becomes smaller and smaller. For C35M alloy, its coefficient of thermal expansion can be described by Eq.(18), as follows:

$$\alpha_{C35M} = (9.81 + 4.53 \times 10^{-3}T - 17.46 \times 10^{-7}T^2 + 9.1 \times 10^{-10}T^3) \times 10^{-6} \quad (18)$$

Terrani et al[24] investigated the temperature creep rate of C35M alloy. Yamamoto et al[21] detected that all the data follow the general power-law creep equation, as follows:

$$\dot{\varepsilon}^{C35M}_{thermal} = A_0\sigma^n \exp\left(\frac{-Q}{RT}\right) \quad (19)$$

where $\dot{\varepsilon}^{C35M}_{thermal}$ is the thermal creep rate (s^{-1}), σ is stress, A_0 is a constant (MPa^{-1}·s^{-1}), and n is the creep exponent. When the temperature is below 970 K, A_0=2.9×10^{-3} MPa^{-1}·s^{-1}, n=5.5, and Q=247 kJ/mol.

The radiation creep rate can be calculated by the following equation[25]:

$$\dot{\varepsilon}^{C35M}_{irr} = 4.5 \times 10^{-31}\sigma\phi \quad (20)$$

Therefore, the creep rate of C35M alloy can be described as follows:

$$\dot{\varepsilon}^{C35M} = \dot{\varepsilon}^{C35M}_{irr} + \dot{\varepsilon}^{C35M}_{thermal} \quad (21)$$

The yield strength of Zr-2 and C35M alloys at different temperatures is shown in Fig.1[21,26].

2 Simulation Framework of Finite Element Method

A small-scale fuel element[27-29] was constructed in ABAQUS software, as shown in Fig.2. The cladding tube has an inner diameter of 4.16 mm and a thickness of 0.57 mm. The length of the simulated tube is 200 mm. The internal fuel is composed of 40 UO_2 pellets to provide the heat source. A gap of 0.07 mm is set between the cladding tube and the fuel pellet. The finite elements C3D8R were used with 10 100 elements in the simulation. One end of the tube is constrained along the axial direction, while the other one is free for axial growth. Furthermore, an additional node along the mid-circumference is constrained at the axial end of the tube in all degrees of freedom to prevent rigid body rotation.

During the manufacturing process, there will be a gap between the fuel pellet and the cladding, and helium gas is added into the gap to improve the heat transfer and protect the structure of the fuel element. Under normal operation conditions, as the temperature of the fuel rod increases and the fission gas is released, the pressure in the gap is increased. In the simulation process, the internal pressure at the initial stage is set as 2 MPa, and it is increased with the procedure proceeding, and finally turns to 10 MPa at the end of the simulation. The outer surface of the cladding is in direct contact with the coolant channel. The pressure on the outer surface of the cladding results from the coolant, which is set as 15.5 MPa and the cooling coefficient is 20 000 W·(m^2·°C)$^{-1}$. According

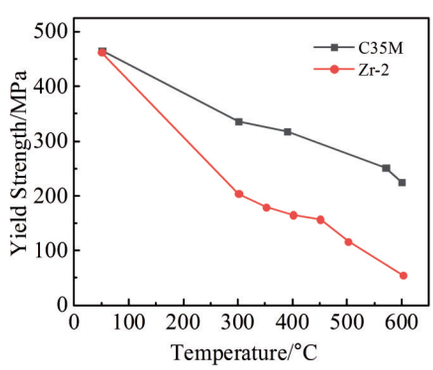

Fig.1 Yield strength of Zr-2 and C35M alloys at different temperatures[21,26]

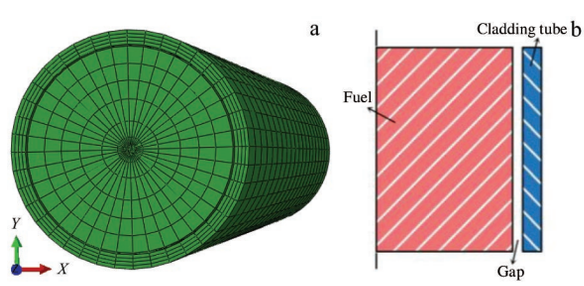

Fig.2 Schematic diagrams of fuel rod (a) and overall model (b) by finite element model

to the actual working conditions of the nuclear power plant, the heat source is 200 W/cm with a flat radial power profile. During the simulation process, the temperature of pellet center rises to 1200 °C in 1 d and the simulated reactor should run in a steady state for 1200 d. In the first 100 d, the fast neutron fluence rate is increased from 0 n· $(mm^2·s)^{-1}$ to $9.5×10^{17}$ n· $(mm^2·s)^{-1}$, and becomes steady until the end of the simulation.

3 Results and Discussion

3.1 Thermomechanical behavior

The temperature field distributions of fuel element at the end of the cladding tube after operation under neutron irradiation for 1200 d are shown in Fig. 3. At the end of the cladding tube, the temperature presents a decreasing gradient distribution from the inner wall to the outer wall. Along the axial direction, the temperature presents a sequential decreasing distribution from the tube end to the middle area. The temperature gradient distribution is caused by the fact that the heat is transferred by the fuel pellets to the inner wall of the cladding, and then to the outer wall of the cladding. Because the outer wall is affected by the coolant and the cooling coefficient of the coolant is large, the temperature of the cladding tubes of two alloys cannot rise continuously and remains at about 312 ° C. This result is consistent with the cladding temperature and the temperature distribution of light water reactor (LWR) fuel rods[12,14,26], indicating the model accuracy.

In order to study the temperature changes of the cladding tubes of two alloys during operation, the data from the outer surface of the fuel pellets and from the inner and outer walls of the cladding tubes are used for analysis, as shown in Fig.4.

The gap and the wire power are important factors to affect the temperature field of the fuel rods. The instantaneous temperature rise at the beginning of the simulation is because the temperature at the middle area of the fuel pellet will rise to 1200 °C within 1 d, as shown in Fig.4. Due to the use of small-sized fuel elements, the heat transfer to the cladding tube will be very fast. The temperature variation trends and temperature change rates of the cladding tubes of the two alloys are basically the same during operation due to their similar thermal conductivities[30]. After the core temperature reaches a

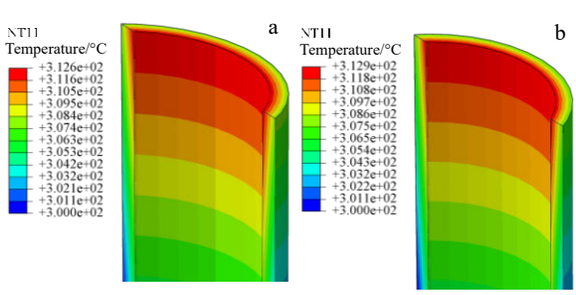

Fig.3 Temperature field distributions of cladding tubes of Zr-2 (a) and C35M (b) alloys

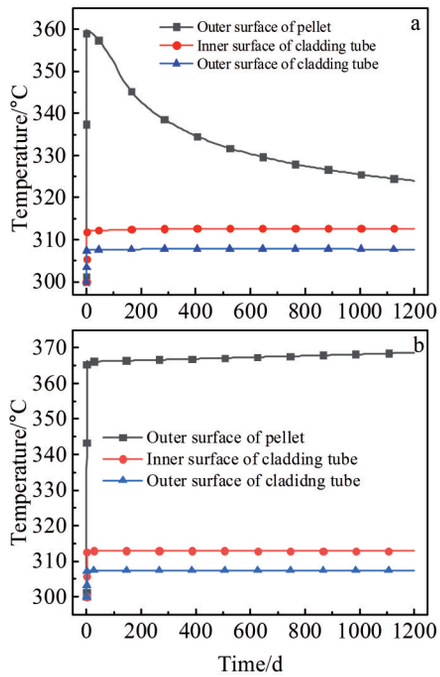

Fig.4 Temperature variations with operation time for cladding tubes of Zr-2 (a) and C35M (b) alloys

stable initial value, the temperature change rate of the cladding tube becomes very slow. The most obvious temperature difference between the two alloy cladding tubes occurs at the outer surface of the UO_2 pellets. This phenomenon is attributed to the fact that the cooling effect of the coolant is affected by the gap distance between the pellet and the cladding tube. Because the irradiated growth does not occur in C35M alloy, the gap of C35M alloy cladding tube will be greater than that of Zr-2 alloy cladding tube, resulting in less influence by the coolant. These results show that the temperature of cladding tube is mainly affected by the line power and coolant rather than the material composition, when the thermal conductivities of the materials are similar to each other.

The stress distribution of the cladding tube is important to evaluate the thermodynamic performance of materials and the safety of fuel elements. The size and distribution of stress on the cladding tube are affected by the temperature and irradiation. In this research, the thermomechanical coupling behavior of the Zr-2 and C35M alloys cladding tubes was studied. The stress field distribution of the two alloy cladding tubes after steady-state operation for 1200 d is shown in Fig.5.

It can be seen from Fig. 5 that the stress field distributions of the two alloy cladding tubes are basically the same, which show the decreasing gradient distribution from the inner wall to the outer wall of the cladding tubes. Both the two alloy cladding tubes meet the structural safety requirements. However, the stress of C35M alloy is twice higher than that of Zr-2 alloy. In the simulation process, since the cladding tubes of the two alloys are not in contact with the fuel pellets, the stress changes are mainly affected by the material properties, cladding temperature, and neutron irradiation. The cladding

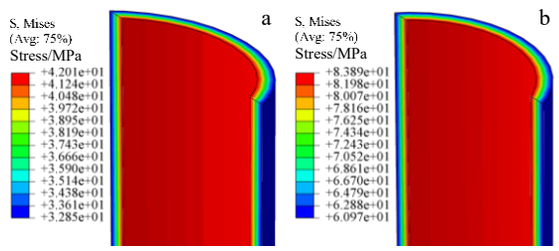

Fig.5 Stress field distributions of cladding tubes of Zr-2 (a) and C35M (b) alloys

temperature and neutron irradiation environment of the two alloys are the same. Thus, different stresses are solely affected by their material properties. In addition, the stress distribution field does not have relationship with the material properties, leading to the fact that the stress depends on the material properties. C35M alloy has a strong radiation resistance, but its creep rate is low. Under severe conditions, with the rapid increase in power, the stress cannot be released. C35M alloy will undergo a sudden change in stress and rupture before Zr-2 alloy. Therefore, in order to adapt to the complex situation in the reactor, the strength of C35M alloy should be further improved.

3.2 Deformation behavior

In the performance simulation of fuel rod, the deformation behavior of the cladding tube and the evolution of the fuel-cladding gap during operation are critical, because they have a significant impact on the fuel temperature and the mechanical properties of the cladding tube. During the simulation, it is considered that the cladding deformation is caused by thermal expansion, thermal creep, radiation creep, and radiation growth. The displacement field distributions of these two alloy cladding tubes after steady-state operation for 1200 d are shown in Fig.6.

It can be observed from Fig. 6 that the displacement fields of Zr-2 and C35M alloys are completely different. The displacement field of Zr-2 alloy cladding tube shows a gradually increasing gradient distribution from the inner wall to the outer wall of the cladding tube, and the displacement distribution is unchanged along the axial direction. The C35M alloy has a gradually decreasing gradient distribution from the inner wall to the outer wall of the cladding tube, and an increasing gradient distribution from the tube end to the middle area can also be observed along the axial direction. The deformation amount of Zr-2 alloy is much greater than that of C35M alloy due to the combination of the hexagonal close-packed crystal structure of the Zr-2 alloy and the texture in the cladding tube. The radiation growth phenomenon occurs during the operation of the reactor[31]. However, the irradiation growth cannot proceed in FeCrAl alloy, i. e., the influence of irradiation growth is slight. Therefore, although the deformation of the Zr-2 alloy cladding tube is affected by thermal expansion, thermal creep, radiation creep, and radiation growth, the deformation is dominated by radiation growth, and the other three deformation mechanisms show slight influence. These results show that C35M alloy exhibits creep deformation and a small amount of thermal expansion deformation due to the restriction of cladding stiffness[32].

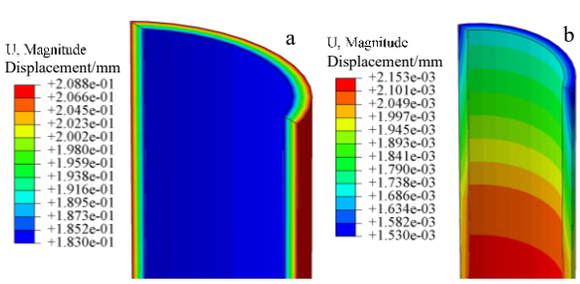

Fig.6 Displacement field distributions of cladding tubes of Zr-2 (a) and C35M (b) alloys

In the displacement field, the deformation distribution of the cladding tubes of two alloys can also be observed. Through the analysis of the displacement field, the processing technique can be optimized for the severely deformed parts of the cladding tube. In order to further determine the pellet-cladding mechanical interaction (PCMI), the radial displacement data of the inner wall of cladding tube and the outer surface of fuel pellet were obtained, and the variation curves of gap distance is shown in Fig.7.

It can be observed from Fig. 7 that the gap closure rate of UO_2-Zr system is much faster than that of UO_2-C35M system. At the beginning of the simulation, the rapid decrease of the gap distance is due to the thermal expansion of the fuel pellets and cladding tube caused by the temperature rise, and then the gap distance is mainly affected by the irradiation. The results show that the dominant deformation mode of Zr-2 alloy cladding tube is irradiation growth, while the creep rate of C35M alloy without irradiation growth is very low, which proves that the application of FeCrAl alloy can greatly delay the gap closure time, prolong the failure reaction time, and prevent the accident. Under the same conditions, the gap closure is largely achieved by fuel expansion as the thermal deformation and radiation creep deformation of C35M alloy are several orders smaller than those of Zr-2 alloy. In order to

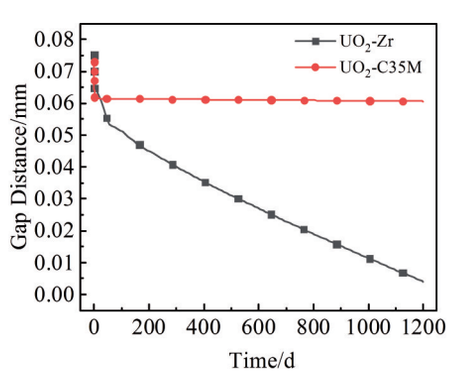

Fig.7 Gap distance variation with operation time between pellet and cladding tubes of Zr-2 (a) and C35M (b) alloys

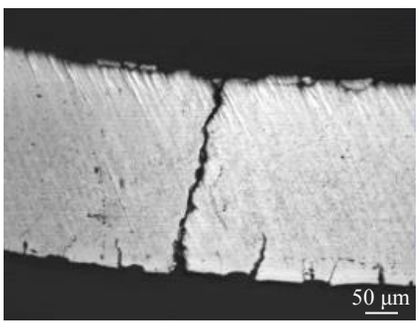

Fig.8 Microstructure of cladding tube failure[33]

produce the same effect as Zr-2 alloy, the fuel particle size and fuel consumption of C35M alloy system should be improved, but the high cost and more fission gas release in the fuel, which will further increase the internal pressure of the cladding tube, restrict the further application. However, the creep rate of FeCrAl alloys is low and the stress cannot be released, which makes the cladding tube easier to crack, as shown in Fig. 8[33]. Therefore, in order to make full use of FeCrAl alloys, it is necessary to modify the gap between the cladding tube and fuel pellet. Moreover, the creep rate and strength of FeCrAl alloys should also be investigated to adapt to the complex conditions in the reactor.

4 Conclusions

1) The temperature distributions and stress field distributions along the radial and axial directions of the C35M and Zr-2 alloy cladding tubes are consistent, showing a gradually decreasing gradient distribution from the inner wall to the outer wall of the cladding tubes. When the thermal conductivities of the two alloys are similar, the temperature is controlled by the cooling coefficient of the coolant. The stress depends on the material properties.

2) The irradiation growth is the main factor for uniform deformation of cladding tube under neutron irradiation. In contrast, the effect of irradiation creep is small. Compared with Zr-2 alloy cladding tube, the gap closure time of C35M alloy cladding tube is longer due to the lack of irradiation growth.

3) The gap distance in FeCrAl alloy cladding tube system should be further improved. In addition, the strength (creep rate and stress) of alloys should be ameliorated in order to prevent the cladding tube from cracking due to the failure of stress release.

References

1 Jiang G Y, Xu D H, Feng P *et al*. *Journal of Alloys and Compounds*[J], 2021, 869: 159 235

2 Adamson R B, Coleman C E, Griffiths M. *Journal of Nuclear Materials*[J], 2019, 521: 167

3 Lemaignan C, Motta A T. *Zirconium Alloys in Nuclear Applications*[M]. Weinheim: Wiley VCH, 2016

4 Terrani K A, Zinkle S J, Snead L L. *Journal of Nuclear Materials* [J], 2014, 448(1-3): 420

5 Ning F Q, Wang X, Yang Y *et al*. *Journal of Materials Science & Technology*[J], 2021, 70: 136

6 Terrani K A. *Journal of Nuclear Materials*[J], 2018, 501: 13

7 Yamamoto Y, Pint, B. A, Terrani K A *et al*. *Journal of Nuclear Materials*[J], 2015, 467(2): 703

8 Huang Xi, Li Xiaoyan, Fang Xiaodong *et al*. *Journal of Materials Engineering*[J], 2020, 48(3): 19 (in Chinese)

9 Bai Guanghai, Xue Fei, Liu Erwei *et al*. *Rare Metal Materials and Engineering* [J], 2020, 49(9): 3071 (in Chinese)

10 Hellstrom K, Hall J, Malmberg P *et al*. *Energy & Fuels*[J], 2014, 28(9): 6116

11 Gao Shixin, Li Wenjie, Chen Ping *et al*. *Nuclear Power Engineering*[J], 2017, 38(5): 175 (in Chinese)

12 Williamson R L. *Journal of Nuclear Materials*[J], 2011, 415(1): 74

13 Qi F Q, Liu Z H, Li Q *et al. Nuclear Engineering and Design*[J], 2020, 367: 110 792

14 Singh G, Terrani K, Katoh Y. *Journal of Nuclear Materials*[J], 2018, 499: 126

15 Li W, Shirvan K. *Journal of Nuclear Materials*[J], 2019, 515: 14

16 Lucuta P G, Matzke H, Hastings I J. *Journal of Nuclear Materials*[J], 1996, 232(2-3): 166

17 Murabayashi M, Tanaka S, Takahashi Y. *Journal of Nuclear Science & Technology*[J], 1975, 12(10): 661

18 Rosinger H E, Northwood D O. *Journal of Nuclear Materials*[J], 1979, 79(1): 170

19 Rashid Y, Dunham R, Montgomery R. *Fuel Analysis and Licensing Code:* FALCON MOD01[R]. Palo Alto: Electric Power Research Institute, 2004: 1 011 308

20 Hoppe N E. *Proceedings of the ANS-ENS International Topical Meeting on LWR Fuel Performance*[C]. Avignon: ANS and ENS, 1991

21 Yamamoto Y, Snead M A, Kevin G *et al*. *Handbook of the Materials Properties of FeCrAl Alloys for Nuclear Power Production Applications*[R]. Oak Ridge: Oak Ridge National Lab, 2017

22 Raju S, Ganesh B J, Rai A K *et al*. *Journal of Nuclear Materials* [J], 2009, 389(3): 385

23 Thompson Z T, Terrani K A, Yamamoto Y *et al*. *Elastic Modulus Measurement of ORNL ATF FeCrAl Alloys*[R]. Oak Ridge: Oak Ridge National Lab, 2015

24 Terrani K A, Karlsen T M, Yamamoto Y. *Input Correlations for Irradiation Creep of FeCrAl and SiC Based on In-Pile Halden Test Results*[R]. Oak Ridge: Oak Ridge National Lab, 2016

25 Chen P, Qiu B W, Wu J M *et al*. *Nuclear Engineering and Design* [J], 2020, 371: 110 889

26 Rao G S, Verma P, Chakravartty J K *et al. Journal of Nuclear Materials*[J], 2015, 457: 330

27 Tang Changbing, Jiao Yongjun, Chen Ping *et al*. *Nuclear Power Engineering*[J], 2017, 38(6): 180 (in Chinese)

28 Xin G, Ding S R, Zhao Y M *et al. Mechanics of Materials*[J], 2013, 65: 110
29 Bell J S, Lewis B J. *Nuclear Engineering and Design*[J], 2012, 250: 134
30 George N M, Terrani K, Powers J *et al. Annals of Nuclear Energy*[J], 2015, 75: 703
31 Gamble K A, Barani T, Pizzocri D *et al. Journal of Nuclear Materials*[J], 2017, 491: 55
32 Sweet R T, George N M, Maldonado G I *et al. Nuclear Engineering and Design*[J], 2018, 328: 10
33 Mishra P, Sah D N, Kumar S *et al. Journal of Nuclear Materials* [J], 2012, 429(1-3): 257

FeCrAl和Zr-2燃料包壳在中子辐照下的热力响应模拟

赵 辉[1]，杨 冲[1]，郭冬旭[1]，吴 璐[2]，潘荣剑[2]，覃检涛[2]，石宝东[1]
(1. 燕山大学 机械工程学院 国家冷轧板带装备及工艺工程技术研究中心，河北 秦皇岛 066004)
(2. 中国核动力研究设计院 第一研究所 核燃料及材料国家重点实验室，四川 成都 610041)

摘 要：选用FeCrAl合金中具有代表性的C35M合金为研究对象，建立小型燃料棒模型，基于用户材料子程序（UMAT），将C35M合金的辐照蠕变模型嵌入子程序中，通过有限元软件ABAQUS计算了其在中子辐照下的热力耦合行为。选用Zr-2合金作为对比，分析了包壳的温度场、应力场、位移场以及间隙距离随时间的演变。结果表明，2种合金的温度场、应力场分布相同，温度分布主要受冷却剂影响，应力场则与温度、蠕变速率有关。在运行过程中，Zr-2合金以辐照生长为主，C35M合金则为辐照蠕变以及少量的热膨胀变形。Zr-2合金的间隙闭合速率远大于C35M合金，这表明C35M合金可以延长事故反应时间，但为了适应反应堆内的复杂环境，材料仍需继续优化，提高其强度以及蠕变速率。

关键词：中子辐照；辐照蠕变；FeCrAl；Zr-2；包壳

作者简介：赵 辉，男，1994年生，博士生，燕山大学国家冷轧板带装备及工艺工程技术研究中心，河北 秦皇岛 066004，E-mail：565366595@stumail.ysu.edu.cn